

Tissue Thermal Property Tomography

Leeor Alon^{1,2}, Christopher Collins^{1,2}, Giuseppe Carluccio¹, Dmitry Novikov¹, Yudong Zhu^{1,2}, and Daniel Sodickson^{1,2}

¹Department of Radiology, Bernard and Irene Schwartz Center for Biomedical Imaging, New York University, New York, NY, United States, ²Sackler Institute of Graduate Biomedical Sciences, New York University, New York, NY, United States

Introduction: In recent years, MR-based methods have been introduced to map the electrical property distribution of tissues inside the body [1,2]. These methods utilize cross-sectional measurements of magnetic fields perturbed by the presence of the body to deduce the spatial distribution of electrical conductivity and permittivity responsible for these perturbations. The Local Maxwell Tomography (LMT) method [2], in particular, uses measurements of field curvature in distinct MR transmit and receive coils to solve for coil-independent tissue- and field-related unknowns based on a self-consistent set of equations. We now propose a related method to reconstruct the distribution of thermal properties of a body from MR thermometry at multiple time points. This method solves Pennes' bio-heat equation [3], rather than Maxwell's equations, and temperature measurements at distinct time points during the body's cooling take the place of measurements of RF field distributions in distinct coils. In this work, theoretical derivations and numerical simulations are presented, showing that thermal properties of a body can be reconstructed by heating an object and measuring spatial and temporal variations in temperature distribution using MR thermometry as the object cools down.

Theory: The Pennes bio-heat equation [3] relates temperature change to perfusion, diffusion, heat capacity and metabolic energy, and can be written as follows in the absence of an external source of heating:

$$\rho c \frac{dT}{dt} = \kappa \nabla^2 T - \rho_{blood} w c_{blood} (T - T_{core}) + Q_m \quad (1)$$

Here, ρ is the density of tissue in kg/m^3 , c is the specific heat capacity in J/kg/C , κ is the thermal conductivity in W/m/C , T is temperature, t is time, w is perfusion in $\text{mL}/100\text{g}/\text{min}$ and Q_m is the metabolic energy generated by the body in W/m^3 . Equation 1 may be discretized in space and in time as described in Ref [4], yielding the following matrix equation, in which each row corresponds to a different acquisition time during cooling:

$$\begin{bmatrix} T_2 - T_1 \\ \vdots \\ T_n - T_{n-1} \end{bmatrix} = \begin{bmatrix} \nabla^2 T_1 dt & \rho_{blood} c_{blood} (T_1 - T_{core}) dt & dt \\ \vdots & \vdots & \vdots \\ \nabla^2 T_{n-1} dt & \rho_{blood} c_{blood} (T_{n-1} - T_{core}) dt & dt \end{bmatrix} \begin{bmatrix} \frac{\kappa}{\rho c} \\ \frac{w}{\rho c} \\ \frac{Q_m}{\rho c} \end{bmatrix} \quad (2)$$

This formalism assumes that heat diffusion, perfusion and metabolic heat terms are time-invariant throughout the experiment. The linear system of equations has a simple solution via matrix inversion, yielding estimates of the heat diffusivity ($\frac{\kappa}{\rho c}$) and the quantities $\frac{w}{\rho c}$ and $\frac{Q_m}{\rho c}$.

Methods and Results: A four channel transmit coil setup around a phantom with 3 different tissue compartments (cerebellum, fat and muscle) was modeled (Figure 1) using commercial FDTD software (xFDTD, Remcom, PA, USA). The voxel size was set to $2.5 \times 2.5 \times 2.5 \text{mm}^3$ and a unit current source was used to drive each of the coils at a frequency of 100MHz. The ex-vivo thermal properties of cerebellum, fat and muscle, as reported in [4], are summarized in Table 1; the greyed area highlights the properties targeted for reconstruction in this work. An RF drive was played out continuously for 200 seconds, inducing a temperature change as shown in Figure 1C for a coronal slice in the center of the phantom. The temperature change due to the RF drive was calculated using a discrete version of the bio-heat equation where the time step size (dt) was set to 2 seconds. After heating, the phantom was allowed to cool down for 2000 seconds and at intervals of 20 seconds a temperature snapshot was taken, as has been shown to be feasible with fast MR thermometry acquisitions [5]. A comparison of true and reconstructed thermal properties is shown in Figure 3.

Discussion and Conclusions: This work lays out a theoretical model allowing the reconstruction of tissue thermal properties based on progressive MR-based temperature measurements. Unlike in the case of LMT, where incomplete measurements of RF magnetic fields require supplementing the set of electrical property unknowns with unknowns such as the absolute RF reference phase, MR thermometry can in principle provide all the interior measurements required to invert the discretized bioheat equation (Eq. (3)) describing the response of the system to thermal perturbation. However, the accuracy of reconstructed maps will depend upon the precision and speed of thermometric acquisitions. Work is underway to reconstruct thermal properties in phantoms and *in vivo* based on rapid MR thermometry measurements.

References: [1] Katscher U et al, IEEE Trans Med Imaging 2009; 28:1365. [2] Sodickson DK et al, ISMRM 2012, p. 387. [3] Pennes HH, J Appl Physiol 1948;1(2):93-122. [4] Collins CM et al, JMIR 2004;19(5):650-656. [5] Cao Z et al. ISMRM 2012, p. 312.

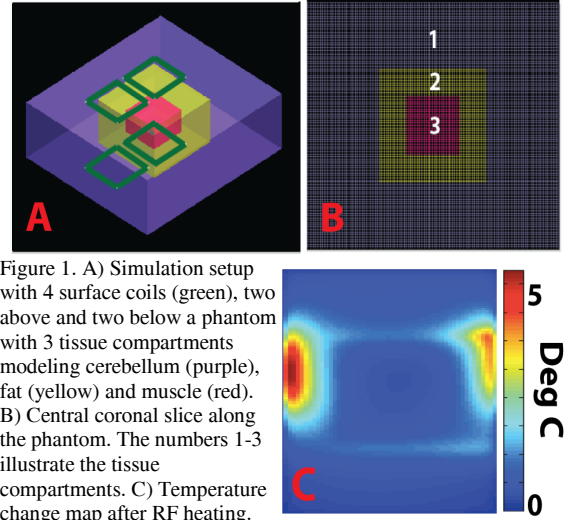


Figure 1. A) Simulation setup with 4 surface coils (green), two above and two below a phantom with 3 tissue compartments modeling cerebellum (purple), fat (yellow) and muscle (red). B) Central coronal slice along the phantom. The numbers 1-3 illustrate the tissue compartments. C) Temperature change map after RF heating.

	ρ (kg/m^3)	c (J/kg/C)	κ (W/m/C)	w ($\text{mL}/100$ g/min)	Q_m W/m^3	$\frac{\kappa}{\rho c}$ (m^2/s)	$\frac{w}{\rho c}$ ($\text{mL} \cdot \text{m}^3 \cdot \text{C} / (100\text{g} \cdot \text{min} \cdot \text{J})$)	$\frac{Q_m}{\rho c}$ (C/s)
Cerebellum	1035.5	3640	0.53	56	331	1.42e-07	1.49e-5	8.78e-5
Fat	943	2300	0.23	2.8	302	1.06e-07	1.29e-6	1.39e-4
Muscle	1059	3500	0.5	5	758	1.34e-07	1.35e-6	2.0e-4

Table 2. Ex-vivo heat-related tissue properties of the simulated phantom.

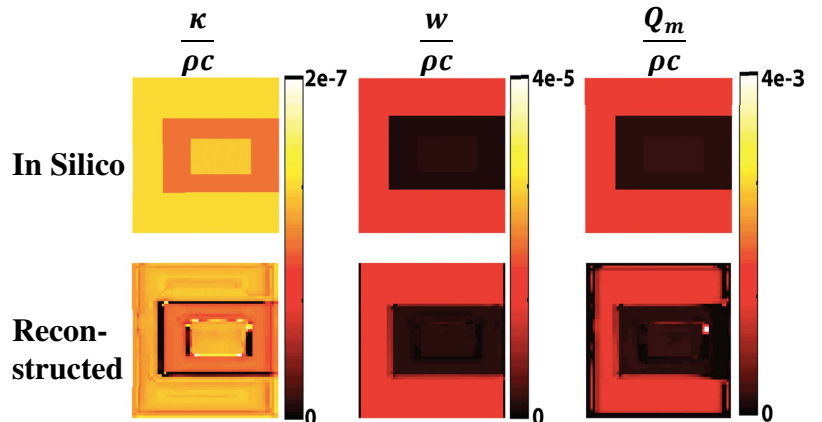


Figure 3. True and reconstructed thermal properties in an axial slice through the phantom.